Proceedings of NHTC'00
34th National Heat Transfer Conferences
August 20-22, 2000, Pittsburgh, Pennsylvania, USA

NHTC2000-12107

CAPILLARY BLOCKING IN FORCED CONVECTIVE CONDENSATION IN HORIZONTAL MINIATURE CHANNELS

Yuwen Zhang, Amir Faghri and Mohammad B. Shafii
Department of Mechanical Engineering
University of Connecticut
Storrs, Connecticut 06269
Email: yuwenz@engr.uconn.edu

ABSTRACT

Capillary blocking in forced convective condensation in a horizontal miniature tube and between parallel plates are investigated numerically. The Volume of Fluid (VOF) method with continuum surface tension model and change of phase is employed to solve the two phase flow. The effects of vapor inlet velocity, saturation temperature, surface tension, and diameter on the condensation length, film thickness and heat transfer coefficient are investigated. The film thickness and the condensation length decrease as hydraulic diameter or the distance between parallel plates decreases. When the total mass flow rate decreases, the condensation length decreases significantly.

NOMENCLATURE

c_p	specific heat, J/kgK
$\mathbf{F}$	body force, N
g	gravitional acceleration, m^2/s
h	sensible enthalpy, J/kg
H	total enthalpy, J/kg
h_c	heat transfer coefficient, W/m^2K
h_{fg}	latent heat, J/kg
$\mathbf{i},\mathbf{j}$	unit vector in x, r (or y) directions
k	thermal conductivity, W/mK
L	length of the tube, m
L_δ	condensation length, m
$\dot{m}''$	mass flux at the interface, kg/m^2s
$\dot{m}'''$	mass source, kg/m^3s
$\dot{m}_t$	total mass flow rate, kg/s
p	pressure, Pa
R	radius of the tube or one half of the distance between parallel plates, m
r	radial coordinate, m
t	time, s
T	temperature, K
u	axial velocity, m/s
v	radial velocity or velocity in y direction, m/s
$\mathbf{V}$	velocity vector, $u\mathbf{i}+v\mathbf{j}$, m/s
x	axial coordinate, m
y	vertical coordinate for parallel plate, m

Greek Symbols

δ	liquid film thickness, m
ε	volume fraction
μ	dynamic viscosity, kg/ms
ρ	density, kg/m^3
σ	surface tension, N/m
σ_0	normal value of surface tension, N/m
∇	gradient operator, $\mathbf{i}\frac{\partial}{\partial x}+\mathbf{j}\frac{\partial}{\partial y}$

Subscripts

in	inlet
ℓ	liquid
sat	saturation
v	vapor
w	wall

INTRODUCTION

It is necessary to develop new cooling strategies for electronic cooling because electronics are becoming more compact and rejection heat flux is increasing. There is a demand for more compact heat transfer devices that are capable of removing large amounts of heat over a small temperature drop. Miniature and micro heat pipes have been and are being used in electronic cooling (Faghri, 1995; 1999). In these

application, the heat generated in the chip is transported away and rejected from the system through condensation. So, in order to optimize the electronic cooling system performance, it is necessary to gain a fundamental understanding of condensation in miniature tubes (Begg *et al.* , 1999).

Flow regimes for two-phase flow in both horizontal and vertical tubes have been studied intensively in the past. However, most flow regime studies on two-phase flow were performed in large diameter tubes (>10 mm i.d.). The distinctive feature of two-phase flow in miniature tubes is that the surface tension may play a significant role in flow pattern transitions. Therefore, the flow regime maps established for conventional sized tube (Mandhane *et al.*, 1974; Taitel and Dukler, 1976) may not apply to two phase flow in miniature tubed because of the role surface tension has on hydrodynamics. So far, the data regarding basic flow patterns for two phase flow with or without heat transfer in miniature circular tubes is still very limited. Barnea *et al.* (1983) presented flow pattern transitions for gas-liquid flow in small diameter tubes (4 to 12mm). They concluded that the effect of surface tension is important for stratified-slug transition in horizontal flow. It should be pointed out these works only dealt with transition of flow patterns without the effect of heat transfer and phase changes.

Condensation in a conventional sized circular tubes have been studied by many scientists. A generally accepted description of forced convection two phase flow patterns in conventional size horizontal tube is presented in Collier and Thome (1994). Depending on orientation of the tube and the mass flow rate, both shear stress on the liquid -vapor interface and the gravitional forces can play important roles on removal of condensate from the tube. Begg *et al.* (1999) reviewed the existing works regarding flow patterns related to condensation and suggested that capillary blocking can occur in miniature tubes. When capillary blocking occurs, the liquid blocks the tube cross section at some distance from the condenser entrance due to capillary force. Both flow visualization and an analytical solution of condensation in miniature tubes were presented. The analytical solution focused on the annular film condensation only and the model could not predict the shape of the meniscus resulted in from complete condensation.

Numerical simulation for two phase devices, such as heat pipe, has advanced significantly during the past decade (Faghri, 1995; 1996). In a conventional heat pipe, evaporation and condensation take place at the interface between the vapor core and the wick, in which case the location of liquid-vapor interface is known *a priori* and the boundary condition at the interface can be easily specified. For condensation in a miniature tube, both the location of the liquid-vapor interface at the film condensation section and the length of the condensation is unknown *a priori* because

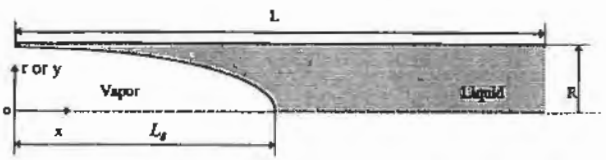

Figure 1. Physical model of condensation in a miniature channel

they are parts of the solution. The numerical method applied in heat pipe simulation is not applicable to predict the capillary blocking in miniature tubes. Volume of Fluid method (VOF; Hirt and Nichols, 1979; Nichols *et al.* , 1980) appeared to be a good candidate because it can be used to determine the location of the interface. The VOF method has been used to simulate a wide range of problems which include vaporization in laser drilling process (Ganesh *et al.* , 1997a; b), solidification in continuons casting (Takata *et al.* , 1999a), and bubble growth in boiling(Takata *et al.* , 1998; 1999b).

The objective of the present effort is to simulate 2-D forced convective condensation in horizontal miniature channels using the VOF method. The interphase mass transfer due to condensation will be considered as a source term in the energy equation. The effect of vapor inlet velocity, wall temperature, saturation temperature, surface tension, and hydraulic diameter on condensation in both miniature tubes and between parallel plates will also be investigated.

PHYSICAL MODEL

The physical model and geometric configuration of the condensation problem in a miniature channel is shown in Fig. 1. The miniature channel can be either a miniature circular tube with a radius of R or two parallel plates $2R$ apart. The saturated vapor enters the channel with a length of L. Condensation takes place on the wall of the channel because the wall temperature, T_w, is below the saturation temperature of the working fluid, T_{sat}. The condensate fluid flows toward the positive x direction due to effect of shear force and surface tension. The problem of interest is condensation in the inner surface of the miniature channel with concurrent vapor flow. It should be noted that the average vapor velocity is not constant along the x direction since condensation occurring on the wall reduces the amount of vapor flow in the core of the tube. The following assumptions are needed in order to solve the condensation problem:

1. Flow both in vapor and liquid phase is laminar and incompressible, and therefore the density for each phase

is constant.

2. The working fluid along the liquid-vapor interface is saturated.
3. The vapor is saturated and therefore there is no temperature gradient in vapor.
4. Since the channel is horizontal and surface tension is dominant, gravitional force is negligible and the liquid film thickness is uniform along the circumferential direction. However, for the cases of Nnsselt condensation and thermosyphon, which are vertical, the effect of the gravity is considered.

When condensation in a conventional sized tube is investigated, the governing equations are often given in Cartesian coordinates since the thickness of the film is significantly smaller than the diameter of the tube (Seban and Faghri, 1985; Harley and Faghri, 1994; Narain *et al.* , 1997). For condensation in miniature tubes, however the thickness of the liquid film is at the same order of magnitude as the diameter of the tube. The governing equations and the corresponding boundary conditions for condensation in miniature circular tubes must be given in cylindrical coordinates. Since forced convection condensation between parallel plates will also be investigated, the governing equations will be written in a generalized from which will be applicable to condensation in both circular tube and between parallel plates.

Governing equations

In order to simplify the solving procedure, one set of governing equations is written for both the liquid and vapor regions. The continuity and momentum equations are

$$\frac{D\rho}{Dt} + \rho \nabla \cdot \mathbf{V} = 0 \tag{1}$$

$$\frac{D\left(\rho \mathbf{V}\right)}{\partial t} = -\nabla p + \nabla \cdot \tau'_{ij} + \mathbf{F} \tag{2}$$

where

$$\tau'_{ij} = \mu \left(\frac{\partial u_i}{\partial x_j} + \frac{\partial u_j}{\partial x_i} \right) + \delta_{ij} \lambda div \mathbf{V} \tag{3}$$

F is the body force resulting from surface tension at the interface, which will be described later. The properties of the liquid-vapor mixture are calculated using

$$\rho = (1 - \varepsilon_v)\rho_\ell + \varepsilon_v \rho_v \tag{4}$$

$$\mu = (1 - \varepsilon_v)\mu_\ell + \varepsilon_v \mu_v \tag{5}$$

where, ε_v is volume fraction of vapor and its value is zero in liquid phase and unity in the vapor phase. For a control volume that includes a liquid -vapor interface, the value of ε_v is between zero and one.

The volume fraction of vapor, ε_v, satisfies the continuity equation of the vapor phase

$$\frac{D\varepsilon_v}{Dt} + \varepsilon_v \nabla \cdot \mathbf{V} = -\frac{\dot{m}'''}{\rho_v} \tag{6}$$

where $\dot{m}'''$ represent represents the mass production rate of condensation.

Equation (6) can be rewritten as

$$\frac{D\varepsilon_v}{Dt} = -\frac{\dot{m}'''}{\rho_v} - \varepsilon_v \nabla \cdot \mathbf{V} = S_{\varepsilon_v} \tag{7}$$

Similarly, the volume fraction of liquid, ε_ℓ, satisfies the following equation

$$\frac{D\varepsilon_\ell}{Dt} + \varepsilon_\ell \nabla \cdot \mathbf{V} = \frac{\dot{m}'''}{\rho_\ell} \tag{8}$$

Substitute eq. (4) into eq. (1) and considering eq. (6), the continuity equation is simplified

$$\nabla \cdot \mathbf{V} = -\left(\frac{1}{\rho_v} - \frac{1}{\rho_\ell} \right) \dot{m}''' \tag{9}$$

Substitute eq. (9) into eq. (7), and obtain the VOF equation

$$\frac{D\varepsilon_v}{Dt} = -\frac{\dot{m}'''}{\rho_v} + \varepsilon_v \dot{m}''' \left(\frac{1}{\rho_v} - \frac{1}{\rho_\ell} \right) = S_{\varepsilon_v} \tag{10}$$

The thermal conductivity and specific heat can be defined using a similar method by which density is defined

$$k = (1 - \varepsilon_v)k_\ell + \varepsilon_v k_v \tag{11}$$

The specific heat is defined using the weight fraction of liquid and vapor

$$c_p = \frac{(1 - \varepsilon_v)\rho_\ell c_{p\ell} + \varepsilon_v \rho_v c_{pv}}{(1 - \varepsilon_v)\rho_\ell + \varepsilon_v \rho_v} \tag{12}$$

The total enthalpy is defined as weighted average of the enthalpy of vapor and liquid phase

$$H = \frac{1}{\rho}\left[\rho_v \varepsilon_v (h_v + h_{fg}) + (1 - \varepsilon_v)\rho_\ell h_\ell\right] \tag{13}$$

Equation (13) can be rearranged as

$$H = h + \Delta H \tag{14}$$

where h and ΔH represent contributions of sensible enthalpy and latent heat on the total enthalpy, i.e.

$$h = \frac{1}{\rho}\left[(1 - \varepsilon_v)\rho_\ell h_\ell + \varepsilon_v \rho_v h_v\right] \tag{15}$$

$$\Delta H = \frac{\varepsilon_v \rho_v h_{fg}}{\rho} \tag{16}$$

The energy equation written in terms of enthalpy and temperature is

$$\frac{D(\rho H)}{Dt} = div\,(k \nabla T) \tag{17}$$

Substituting eq. (16) into eq. (17), one can obtain

$$\frac{D(\rho h)}{Dt} = div\,(k \nabla T) + S_{\Delta H} \tag{18}$$

where

$$S_{\Delta H} = -\left[\frac{\partial}{\partial t}\rho \Delta H + \nabla \cdot (\rho \Delta H \mathbf{V})\right] \tag{19}$$

It can be seen that an additional term appears on the right hand side of eq. (18). This term accounts for the effect of condensation in the energy equation.

Substituting eq. (15) into eq. (19) leads to

$$S_{\Delta H} = -\left[\frac{D(\varepsilon_v \rho_v h_{fg})}{Dt} + \varepsilon_v \rho_v h_{fg} \nabla \cdot \mathbf{V}\right] \tag{20}$$

For incompressible flow, the density of vapor is a constant, eq. (20) is simplified

$$S_{\Delta H} = -\rho_v h_{fg}\left(\frac{D\varepsilon_v}{Dt} + \varepsilon_v \nabla \cdot \mathbf{V}\right) \tag{21}$$

Compare eq. (6) and eq. (21); the mass production rate due to condensation, $\dot{m}'''$, is related to the source term in the energy equation, $S_{\Delta H}$, using

$$\dot{m}''' = \frac{S_{\Delta H}}{h_{fg}} \tag{22}$$

Boundary conditions

The inlet condition for both the circular tube and parallel plates can be written as

$$u = \begin{cases} u_{in,v} & 0 < r < R - \delta, \quad x = 0 \\ u_{in,\ell} & R - \delta < r < R, \quad x = 0 \end{cases} \tag{23}$$

$$v = 0, \quad x = 0 \tag{24}$$

$$T = T_{sat}, \quad x = 0 \tag{25}$$

The boundary conditions at the wall are

$$u = v = 0, \quad r = R \text{ (tube) or } y = R \text{ (parallel plates)} \tag{26}$$

$$T = T_w, \quad r = R \text{ (tube) or } y = R \text{ (parallel plates)} \quad (27)$$

The boundary condition at exit of the computational domain can be written in a generalized form: $\partial\phi/\partial x = 0$ at $x = L$, where ϕ can be u, v, or T. The boundary conditions along the line of symmetry can be expressed as $\partial\phi/\partial r = 0$ at $r = 0$ for circular tube, or $\partial\phi/\partial y = 0$ at $y = 0$ for parallel plates.

Consideration of liquid-vapor interface

The conservation of normal and tangential momentum for the control volumes at the solid-liquid interface is automatically satisfied because the governing equations were written for the entire computational domain, including liquid and vapor. The pressure jnmp conditions at the liquid vapor interface due to surface tension need to be taken into account. The effect of surface tension on pressure is modeled using continues surface model. The model interprets surface tension as a continuous, 3-D effect across the interface, rather than a boundary condition on the interface (Brackbill *et al.* , 1992). Forces due to the pressure jump at the interface can be expressed as volume force using the divergence theorem

$$\mathbf{F} = 2\sigma K \epsilon_\ell \nabla \epsilon_\ell \quad (28)$$

where curvature of the interface, K, is given by (Brackbill *et al.*, 1992)

$$K = \frac{1}{|\mathbf{n}|}\left[\left(\frac{\mathbf{n}}{|\mathbf{n}|}\cdot\nabla\right)|\mathbf{n}| - (\nabla\cdot\mathbf{n})\right] \quad (29)$$

The normal direction of the liquid- vapor interface toward vapor phase is $\mathbf{n}$. It can be seen that the body force, F, will be zero everywhere except for the control volume that includes the interface. The body force , F, obtained by eq. (28) is substituted into the momentum equation (2) to solve for the velocities in the liquid and vapor phases.

Liquid and vapor temperature are continuous at the interface. Therefore, the temperature at the liquid -vapor interface is expressed as

$$T = T_{sat} \quad (30)$$

where T_{sat} is saturation temperature.

The energy balance at the liquid vapor interface also needs to be satisfied. Since liquid and vapor regions are treated as one domain, the energy balance at the liquid vapor interface is satisfied when the converged solution for the entire domain is obtained.

A NUMERICAL TECHNIQUE TO DETERMINE THE SOURCE TERMS

At the liquid -vapor interface, the temperature is equal to the saturation temperature as stated in eq. (30). The enthalpy corresponding to the above interface temperature is

$$h = c_p(T_{sat} - T_{ref}) \quad (31)$$

where T_{ref} is the reference temperature defined as the temperature at which the enthalpy is zero.

In order to set the temperature and enthalpy at the interface to the above values, the following source term is introduced into the enthalpy equation

$$S_{\Delta H} = A + Bh \quad (32)$$

with $A = 10^{10} c_p(T_{sat} - T_{ref})$ and $B = 10^{10}$ for the cells with ϵ between 0 and 1. By doing this, the numerical solution will yield eq. (30) and (32). This is a numerical technique to set the value of temperature and enthalpy values at the interface.

After the temperature at the interface is set to T_{sat} by the above technique, eq. (18) is used to determine the $S_{\Delta H}$

$$S_{\Delta H} = \frac{D(\rho h)}{Dt} - div\,(k\nabla T) \quad (33)$$

The mass source $\dot{m}'''$ for VOF equation and continuity equation is then determined eq. (22).

NUMERICAL SOLUTION PROCEDURE

Here, only steady state solution of the condensation problem is investigated. It is impossible to solve the steady state problem directly, because the donor-acceptor model used in the VOF method works only for unsteady state problem. A false transient method (Basu and Srinivasan, 1988) is employed. With this methodology, the false transient terms are included in the governing equations and

steady state is obtained when the condensation length does not vary with the false time. In order to accelerate convergence, the initial VOF distribution in the channel for a specific case can be set as the converged VOF distribution for a similar case. Numerical experiments on the effect of initial VOF distribution on the final results are performed for several cases. It is found that the final results are the same for different initial VOF distributions which means that the final results are not influenced by initial conditions. The overall numerical solution procedure for a particular time step is outlined below:

1. Assume a value for the mass production rate, $\dot{m}'''$ and compute the source term for the VOF equation (10) and the continuity equation (9).
2. Solve the VOF eq. (10).
3. Solve the continuity equation and momentum equations.
4. Solve for the temperature distribution from eq. (18). For the control volumes including the interface, the temperature is set to the saturation temperature and eq. (22) is used to determiue the mass production rate, $\dot{m}'''$.
5. Compute the source term for the VOF equation (10) and the continuity equation (9).
6. Go back to step 2 until the relative residuals for the pressure correction equation, momentum equations, and enthalpy equation are within the limit.

After the solution for the current time step is obtained, the computation for the next time step is performed. The above numerical procedure is implemented in a commercial package (Fluent Inc., 1998). Although the VOF method has been employed in Fluent to simulate multiphase flow with a free surface, the interphase mass transfer model was not available, so that the evaporation and condensation phenomena cannot be simulated directly using Fluent. In order to simulate condensation in miniature channels using Fluent, the interface mass transfer is modeled using a customized user defined code. This code is compiled and linked with the remaining Fluent objects code to create a new customized executable file.

RESULTS AND DISSCUSION

Verification

In order to verify the numerical method and code, Nusselt condensation of steam vapor on a vertical flat plate is solved. The vapor is assumed to be at the saturation temperature (363K) and the wall temperature is 340K. The

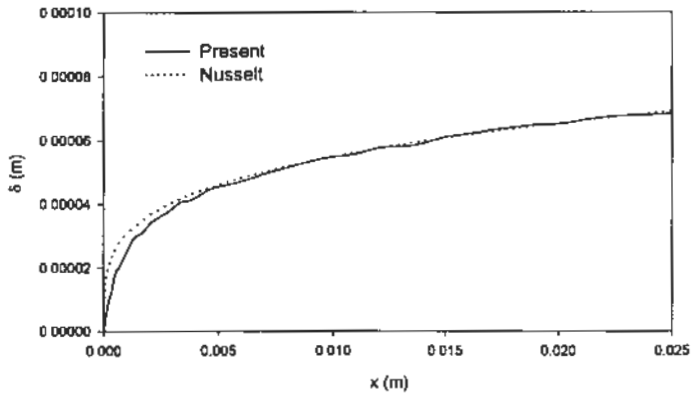

Figure 2. Comparison of liquid film thickness for Nusselt Condensation

effect of gravity is included in the model since it is dominant for the vertical plate. The comparison of liquid film thickness obtained by present model to the Nusselt analysis is presented in Fig. 2. It can be seen that the interface obtained by the present method is not very smooth, which is due to the limitation of the donor-acceptor mothod used to solve the VOF equation (Takata et al., 1999). However, the overall agreement between the present result and the Nusselt analysis is still very good.

Forced film condensation on a horizontal flat plate (Fig. 3a; Shekriladze and Gomelauri, 1966) is then solved. The working fluid is R-113, and the velocity and saturation temperature of vapor at infinity is assumed to be 0.3m/s and 320.57 K. The temperature at the surface of the plate is chosen to be 310.56 K. Fig. 3(b) shows the comparison of the film thicknesses obtained by the present numerical solution and the approximate solution by Shekriladze and Gomelauri (1966). The agreement between the present results and that of Shekriladze and Gomelauri (1966) is fairly good up to 1 cm from leading edge. The discrepancy between the present results and the that of Shekriladze and Gomelauri (1966) for larger x can be explained using the shear stress model used in Shekriladze and Gomelauri (1966). The shear stress at the liquid vapor interface is calculated using

$$\tau_0 = j\,(U_\infty - U_s) \tag{34}$$

where j is mass flow rate of vapor at the liquid-vapor surface due to condensation, and U_s is velocity at the liquid vapor interface. The shear stress caused by the gradient of the horizontal velocity was neglected, and the shear stress on the liquid-vapor interface was assumed to be dependent ou the momentum change due to suction at the interface. This

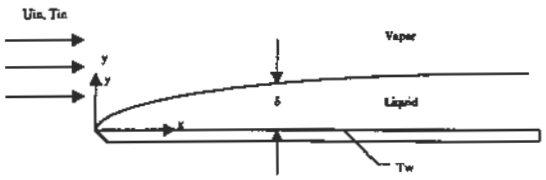

(a) Physical model

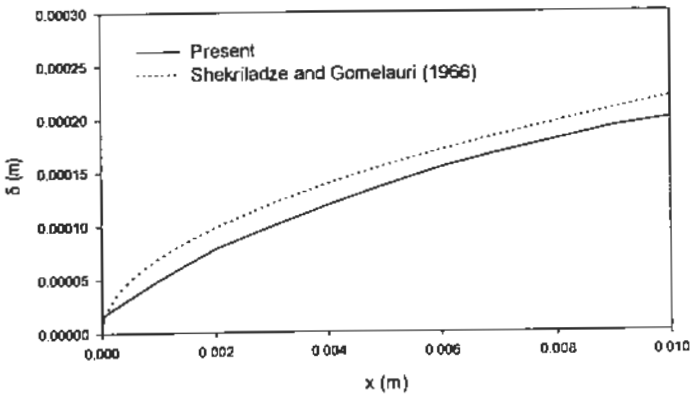

(b) Comparison with Shekriladze and Gomelauri (1966)

Figure 3. Forced convective film condensation

becomes more accurate when the film thickness is very small and the condensate rate is very high. As the film thickness increases, the rate of condensation decreases, and consequently the momentum transferred by the suction mass at the interface decreases. Eventually the momentum transferred by the suction mass is no longer significant, and the shear stress on the liquid-vapor interface depends on the momentum changes due to the velocity gradient and the suction due to condensation. Therefore Shekriladze and Gomelauri's (1966) approximate solution overestimates the film thickness for larger x.

Another verification of the numerical method was performed by simulating the condensation in a condenser section of a thermosyphon (Seban and Faghri, 1984). The geometric configuration of the problem is similar to Fig. 1, except the tube is closed at $x = 0$ and the effect of gravity must be taken into account. The tube is vertieal, and the gravity acts in the positive x direction. Vapor flows toward the negative x direction, but the liquid flows toward the positive x direction due to the effect of gravity. For the complete problem description see Seban and Faghri (1984). The radius and the length of the circular tube are $R = 1.21$ mm and $L = 4.0$ cm, respectively. The working fluid is methanol with a saturation temperature of $336K$ and a wall temperature of $310.8K$. The numerical results are compared with the analytical results of Seban and Faghri (1984), and the present results are shown in Table 1. The agreement between the present results and Seban and Faghri (1984) is very good. Also evident from Table 1 is that the effect of surface tension is not significant for this case, because the process is mainly dominated by gravity.

Table 1 Comparison of present results with the resnlts of Seban and Faghri (1984)

	Re_v	Re_ℓ	$\delta\|_{x=L}$	$\overline{Nu}$
Nusselt Analysis				18.1
Seban and Faghri (1984)	495	3.3	2.78×10^{-4}	38.4
Present ($\sigma = 0$)	510	3.42	2.69×10^{-4}	39.6
Present ($\sigma = 19.03mN/m$)	530	3.51	2.60×10^{-4}	41.1

Condensation in a miniature circular tube

The condensation in horizontal miniature tubes as shown in Fig. 1 is then investigated. The radius and the length of the tube is R=1.5 mm, L=2cm, respectively. The working fluid is water with a saturation temperature of 363K or 323K. The inlet temperature is always equal to the saturation temperature. The difference between the wall temperature and saturation temperature is 23K for all cases. The thermal properties of the working fluid can be found in Faghri (1995) and will not be repeated here. After the grid size and the time step test, the problem is solved using a non-uniform grid of $42(x) \times 32(r)$. The grid near the wall is very fine in order to simulate fluid flow in the liquid layer. The grid at small x is very fine in order to simulate the closed condensation phenomena. After several numerical tests, the false time step used in the computation is $\Delta t = 10^{-6}s$.

Fig. 4 shows the volume fraction of water at different vapor inlet velocities. The dark area in the figure is vapor and the gray area is liquid. The light area that exists between the liquid and vapor region is the liquid-vapor interface. The total mass flow rate of liquid and vapor for both cases are $\dot{m}_i = 10^{-5}kg/s$, and the liquid film thickness at the entrance of the tube is 0.08 mm (Begg et al., 1999). The capillary blocking phenomenon occurred for both cases. For the case with vapor inlet velocity of 1.244 m/s, the condensation length measured at the center of the tube is 4.7 mm. When the vapor inlet velocity is reduced by half, the condensation length is reduced to 3.1 mm.

Fig. 5 shows the VOF for water when the saturation temperature is reduced to 323K. The mass flow rate of vapor in Fig 5 (a) and (b) is the same as the mass flow rate of vapor in Fig. 4 (a) and (b). Since the density of vapor

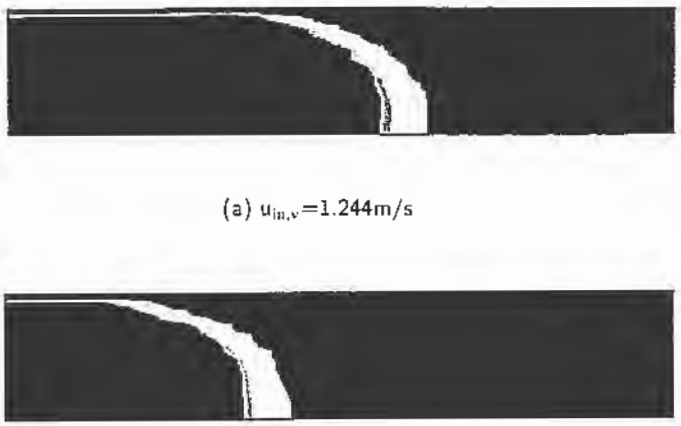

(a) $u_{in,v}$=1.244m/s

(b) $u_{in,v}$=0 622m/s

Figure 4. Contour of vapor VOF at different vapor inlet velocities ($\dot{m}_t$= $10^{-5}kg/s$, $T_{sat} = 363K$, $T_w = 340K$)

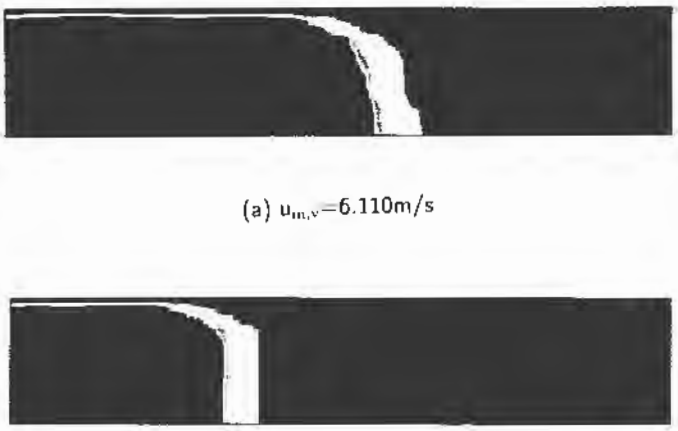

(a) $u_{in,v}$=6.110m/s

(b) $u_{in,v}$=3.055m/s

Figure 5. Contour of vapor VOF at different vapor inlet velocities ($\dot{m}_t$= $10^{-5}kg/s$, $T_{sat} = 323K$, $T_w = 300K$)

at 323 K is significantly lower than that at 363K, the vapor inlet velocities in Fig. 5 are significantly higher than those for Fig. 4. As shown in Fig. 5, the liquid film is not smooth due to the shear force induced by the high vapor velocity. The condensation lengths for two cases are 4.6 mm and 2.7 mm respectively. Compared with the condensation length in Fig. 4, the condensation length is not strongly affected

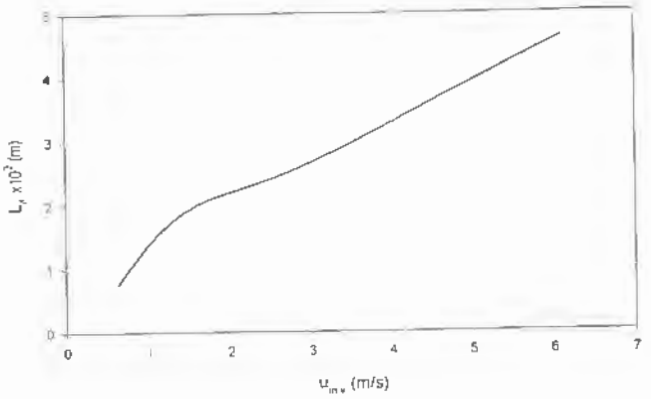

Figure 6. Effect of vapor inlet velocity on the condensation length ($\dot{m}_t$ $10^{-5}kg/s$, $T_{sat} = 323K$, $T_w = 300K$)

by the saturation temperature. For same mass flow rate of vapor, the condensation lengths at different saturation temperature are very close. The effect of vapor inlet velocity on the condensation length for a saturation temperature of 323K is shown in Fig. 6. The total mass flow rate remains at $\dot{m}_t$= $10^{-5}kg/s$ for different vapor inlet velocities. The condensation length increases sharply when the vapor inlet velocity is small. The condensation length however becomes a linear function of vapor inlet velocity after the vapor inlet velocity is greater than 2.5 m/s. The velocity vectors corresponding to the case in Fig. 4(a) and Fig. 5(a) are shown in Fig. 7(a) and (b). As mentioned before, the mass flow rates for Fig. 7(a) and (b) are the same although the vapor inlet velocities are different. Since condensation occurred on the wall, the vapor velocity vectors near the wall point to the wall. The mean vapor velocity decreases with x due to condensation.

Fig. 8(a) shows the variation of liquid film thickness for the cases in Fig. 4(a) and (b). It can be seen that the behavior of liquid film thickness is different for different vapor inlet velocities. When the vapor inlet velocity is low, the film thickness is almost constant before it increases sharply to block the tube. When the vapor inlet velocity is higher, the film thickness along most of the effective condensation length is constant. There is however a film thickness decrease before the sharp increase, which agrees with Begg *et al.* (1999). The heat transfer coefficient based on the difference between saturation temperature and wall temperature corresponding to Fig. 8(a) is shown in Fig. 8(b). It can be seen that the heat transfer coefficient along the condensation length is very high but decreases sharply when capillary blocking occurs. For the case of high vapor inlet velocity,

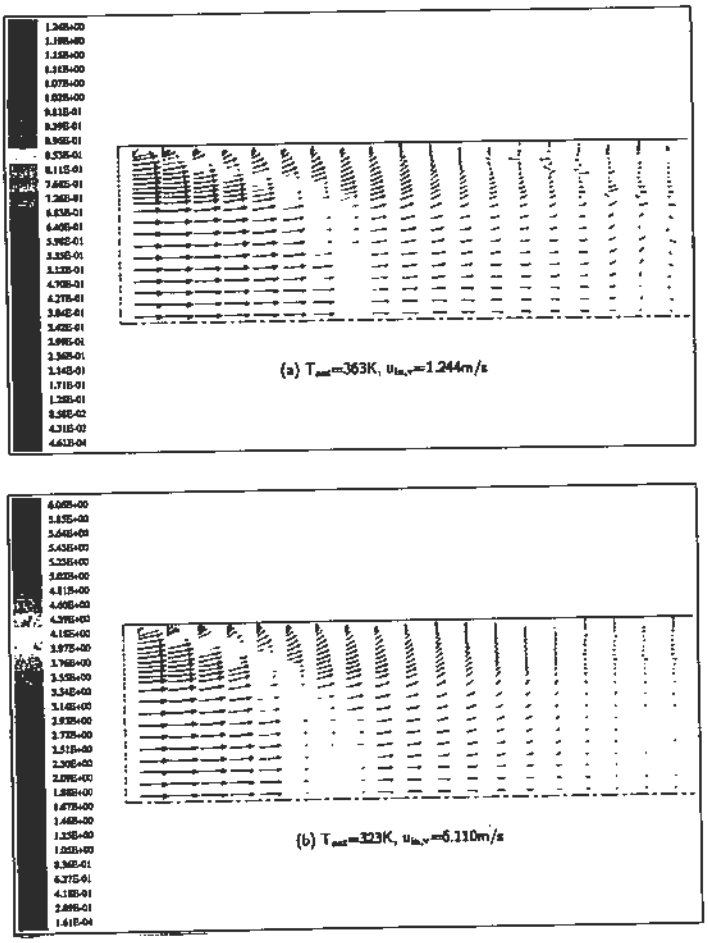

Figure 7. Velocity vectors at different saturation temperature for miniature tube

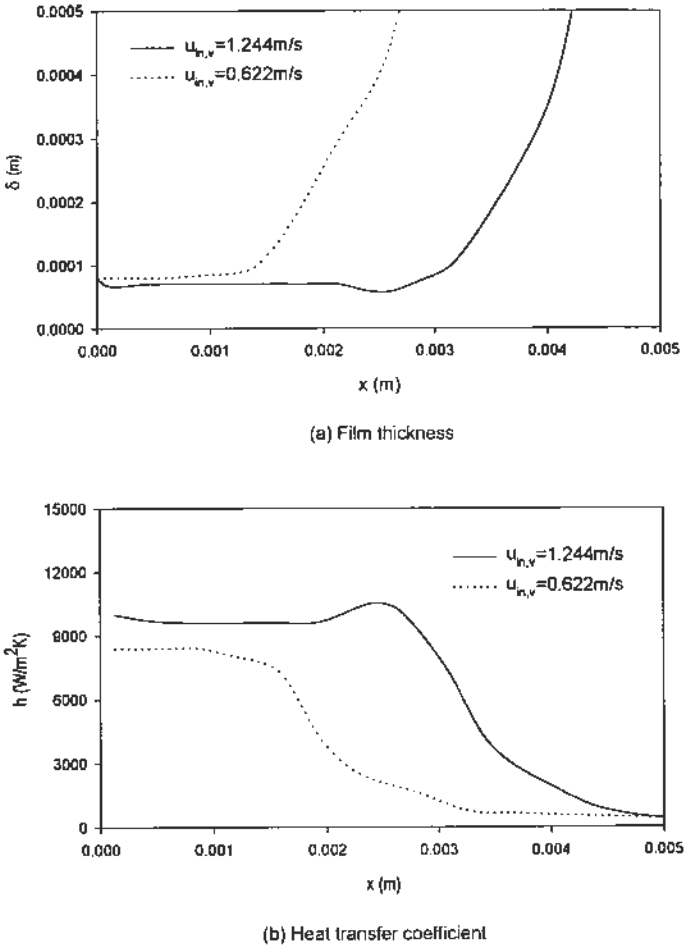

Figure 8. Effect of vapor inlet velocity on condensation in miniature tubes ($\dot{m}_l = 10^{-5} kg/s$, $T_{sat} = 363K$, $T_w = 340K$)

the heat transfer coefficient before capillary blocking is very high because the liquid film is thinner at this location.

The variations of liquid film thickness corresponding to the cases in Fig. 5(a) and (b) are shown in Fig. 9(a). The liquid film thickness decreases first and then increases. Before capillary blocking occurs in the tube, there is a decrease in liquid film thickness. This wavy shape of liquid film shown is due to the shear force caused by high vapor velocity. The heat transfer coefficients corresponding to Fig. 9(a) are shown in Fig. 9(b). It can be seen that the heat transfer coefficients in the condensation length also show wavy shapes due to variation in liquid film thickness.

The effect of surface tension on the liquid film thickness and condensation length for the vapor inlet velocity of 1.244 m/s is shown in Fig. 10(a). In addition to the result for surface tension at its normal value, σ_0, two curves with changed surface tensions but same mass flow rates are also plotted in Fig.10(a) for comparison. It can be seen that the condensation length decreases with increasing the surface tension, which is in agreement with (Begg *et al.* 1999). Increasing the surface tension thins the liquid film thickness, and therefore condensation rate within the condensation length increases. Consequently, the condensation length required to condense the same amount of vapor decreases. The reason that film thickness thins with increasing surface tension is that the condensation phenomenon always tends to minimize the surface energy at the interface. With increasing the surface tension this energy increases. In order to reduce this energy the radii of curvature has to be increased and that means liquid film thickness has to be decreased. Fig. 10(b) shows the heat transfer coefficient along the tube for varying surface tension. The maximum heat transfer coefficient value within the condensation length is obtained from

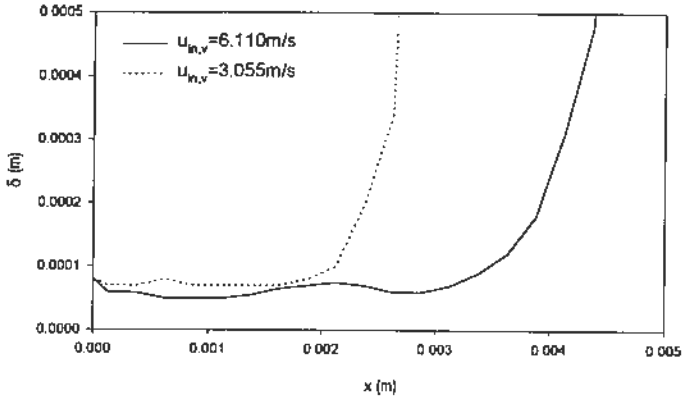

(a) Film thickness

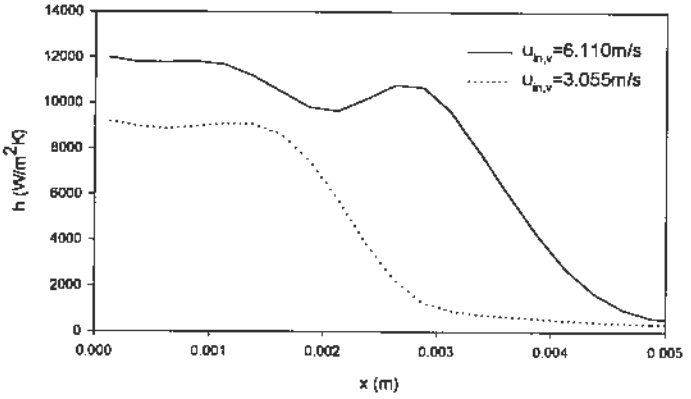

(b) Heat transfer Coefficient

Figure 9. Effect of vapor inlet velocity on condensation in miniature tubes ($\dot{m}_t$= $10^{-5}kg/s$, $T_{sat} = 323K$, $T_w = 300K$)

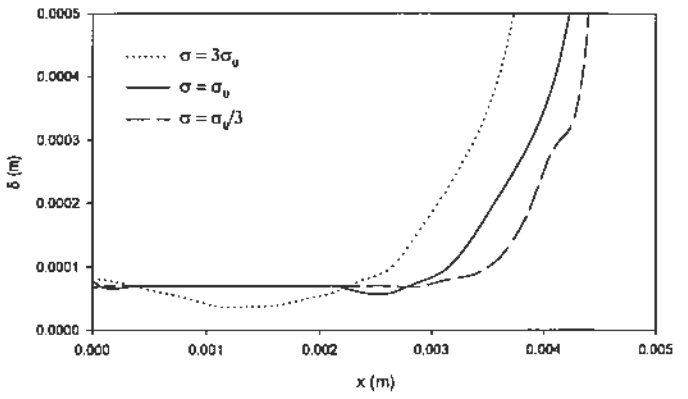

(a) Film thickness

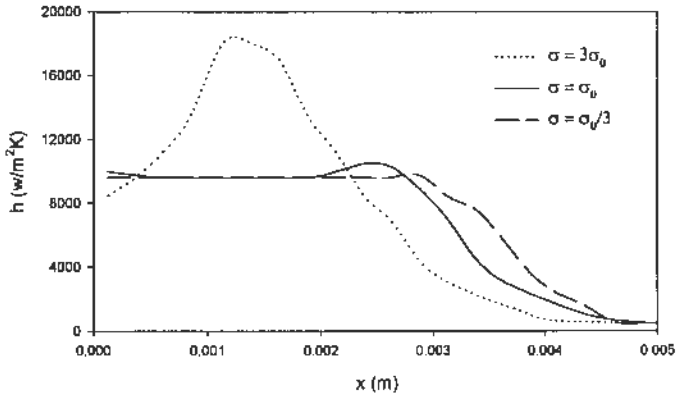

(b) Heat transfer coefficient

Figure 10. Effect of surface tension on condensation in miniature tubes ($\dot{m}_t$= $10^{-5}kg/s$, $u_{in,v} = 1.244m/s$, $T_{sat} = 363K$, $T_w = 340K$)

the case with the highest surface tension. In this case average heat transfer coefficient is greater than the others. This is consistent with the expectation that higher total average heat transfer coefficient leads to a shorter condensation length.

The effect of the radius of the miniature tube on film thickness and the heat transfer coefficient is shown in Fig. 11. The inlet velocities of both liquid and vapor for three cases presented in Fig. 11 are the same, and therefore the total mass flow rate for smaller diameter tube is lower. As can be seen from Fig. 11 (a), the liquid film thickness decreases with decreasing tube diameter, because the surface tension plays a more important role. The condensation length also decreases with decreasing tube diameter, because the total mass flow rate decreases with decreasing tube diameter. Fig. 11(b) shows the effect of tube diameter on the heat transfer coefficient. It is seen that the heat transfer coefficient within the condensation length is significantly higher for smaller diameter tubes, because the liquid film is thinner.

The effect of total mass flow rate on condensation in circular miniature tubes is also investigated and the results are shown in Fig. 12. In addition to the reference case ($\dot{m}_t$= $10^{-5}kg/s$), the results for the reduced total mass flow rate are shown in Fig. 12. It can be seen from Fig. 12(a) that the film thickness is significantly increased and the condensation length is significantly decreased with decreasing total mass flow rate. Consequently, the heat transfer coefficient is significantly decreased when the total mass flow rate is reduced by one order of magnitude.

Condensation between parallel plates

Condensation phenomena in miniature channels formed by two parallel plates are also investigated. The distance be-

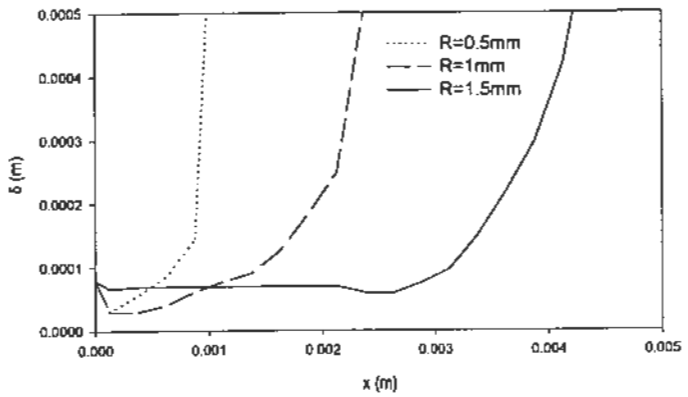

(a) Film thickness

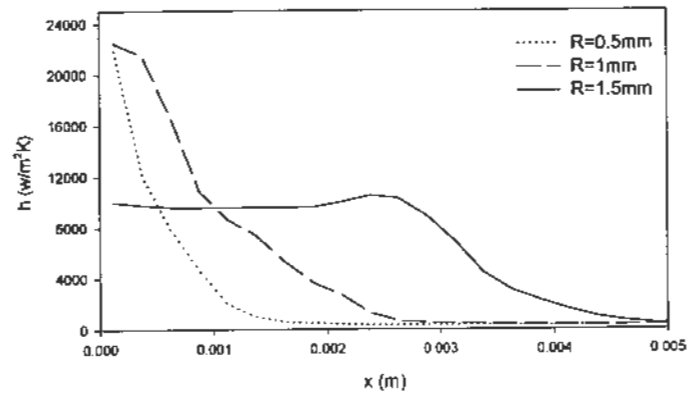

(b) Heat transfer coefficient

Figure 11. Effect of diameter on the condensation in miniature tubes ($u_{in,v} = 1.244m/s$, $T_{sat} = 363K$, $T_w = 340K$)

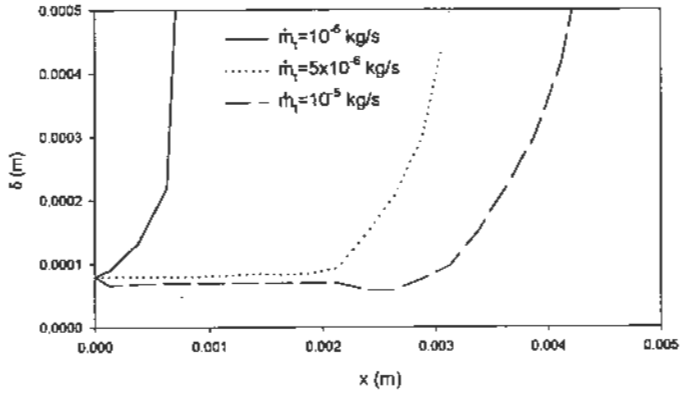

(a) Film thickness

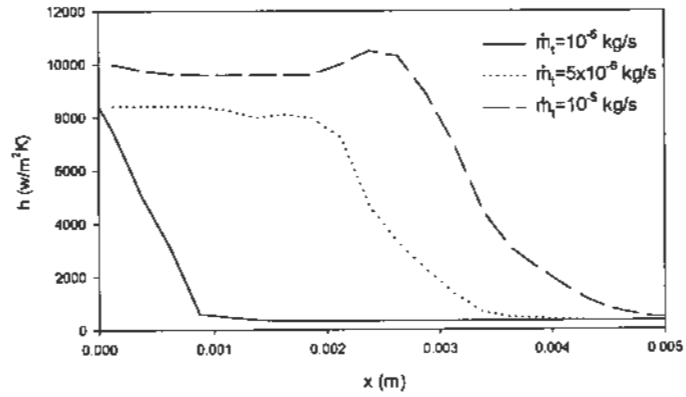

(b) Heat transfer coefficient

Figure 12. Effect of total mass flow rate on the condensation in miniature tubes ($R = 1.5mm$, $T_{sat} = 363K$, $T_w = 340K$)

tween plates and the length of the channel are: $2R = 3mm$ and $L = 2cm$, respectively. The effect of gravity is neglected and therefore this is a axisymmetric problem about $y = 0$. Only half of the domain ($0 < y < R$) therefore is solved. A non-uniform grid of $42(x) \times 32(y)$ with a time step of $\Delta t = 10^{-6}$ is used to solve this problem. Fig. 11(a) shows the variation of liquid film thickness along the horizontal parallel plates for different vapor inlet velocities. The total mass flow rate of liquid and vapor for both cases is $\dot{m}_t = 8.3 \times 10^{-4} kg/(ms)$. It is seen that the condensate film thins close to the blocking point for both high ($u_{in,v} = 0.62\ m/s$) and low ($u_{in,v} = 0.2m/s$) vapor inlet velocities. The variation of the liquid film thickness is different for two different velocities. For lower vapor inlet velocity, film thickness decreases in positive x direction up to the blocking point due to the shear stress and surface tension at the blocking point where the curvature of interface is large. For higher vapor inlet velocities, the film is thin and tends to be wavy due to the higher shear stresses. These variations of liquid film thickness was not observed for the circular tube because the surface tension due to the curvature of the tube radius can suppress the wave in the tube. The heat transfer coefficients for the cases corresponding to Fig. 11(a) are shown in Fig. 11(b). The heat transfer coefficients are highest before the blocking point, where the rate of condensation is highest.

The effect of surface tension on film thickness and the condensation length is shown in Fig. 12(a). The vapor inlet velocity for all three cases is $0.2m/s$. As can be seen from Fig. 12(a), the condensation length decreases with the increasing surface tension. When the surface tension increases, the liquid film thickness becomes thinner at the locations closest to the blocking point. The heat transfer coefficients along the plates for different values of surface

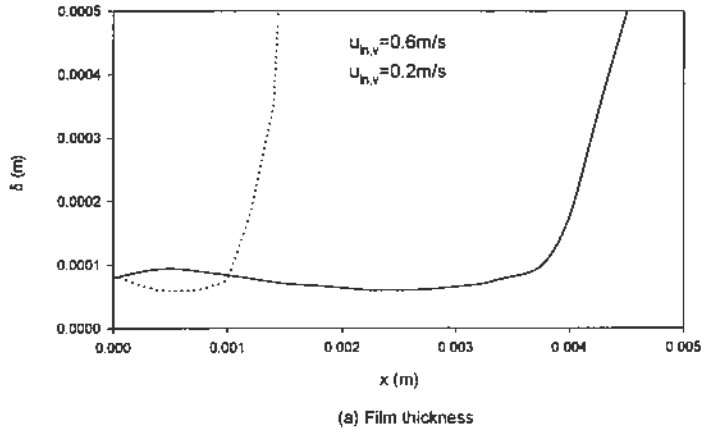

(a) Film thickness

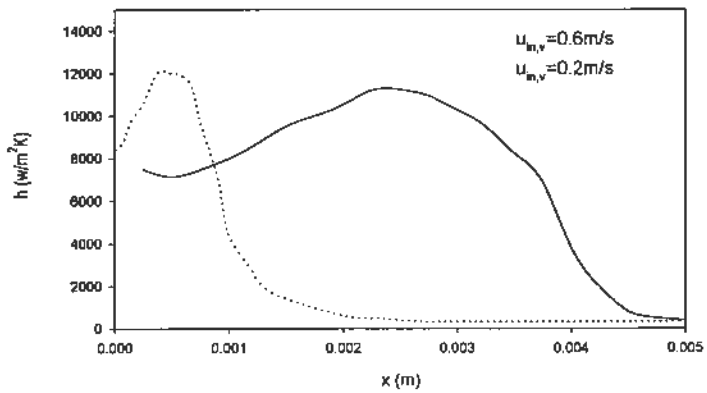

(b) Heat transfer coefficient

Figure 13. Effect of vapor inlet velocity on condensation between parallel plates ($\dot{m}_t$= $8.3 \times 10^{-4} kg/ms$, $T_{sat} = 363K$, $T_w = 340K$)

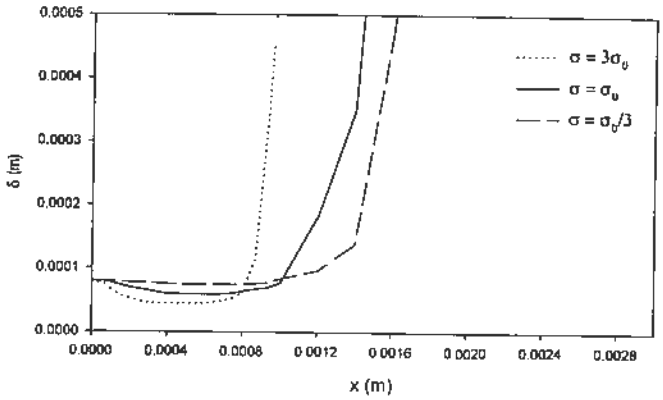

(a) Film thickness

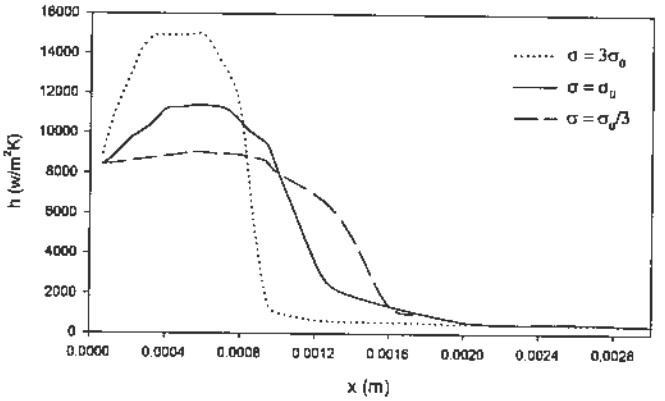

(b) Heat transfer coefficient

Figure 14. Effect of surface tension on condensation between parallel plates ($\dot{m}_t$= $8.3 \times 10^{-4} kg/ms$, $u_{in,v} = 0.2m/s$, $T_{sat} = 363K$, $T_w = 340K$)

tension are shown in Fig. 12(b). It is observed that the total average heat transfer coefficient for all cases is the same, because the vapor inlet velocities are the same.

Fig. 15 shows the effect of the distance between parallel plates on condensation. The inlet velocities of liquid and vapor for different distances are the same, which means that the total mass flow rate for smaller distances between parallel plates is lower. It can be seen from Fig. 15(a) that the liquid film thickness is slightly decreased when the distance between parallel plates is decreased, which is different from the behavior in circular tubes because surface tension is less important for condensation between parallel plates. The condensation length is decreased with decreasing distance between parallel plates, because the total mass flow rate is lower for smaller distances between parallel plates.

CONCLUSIONS

Numerical simulation for condensation in horizontal miniature circular tubes and between parallel plates with capillary blocking is performed using VOF method. The effect of various physical and geometric parameters on liquid film thickness, condensation length, and heat transfer coefficients for both circular tube and parallel plates are investigated. The results show that the condensation length increases sharply with increasing vapor inlet velocity when the vapor velocity is small. When the inlet vapor velocity is higher, the condensation length is a linear function of inlet vapor velocity. The condensation lengths for different saturation temperatures are very close for same mass flow rate of vapor. The liquid film thickness is smooth for lower vapor velocities. The wavy shape of the liquid film was observed for the cases with high vapor velocity. When the surface

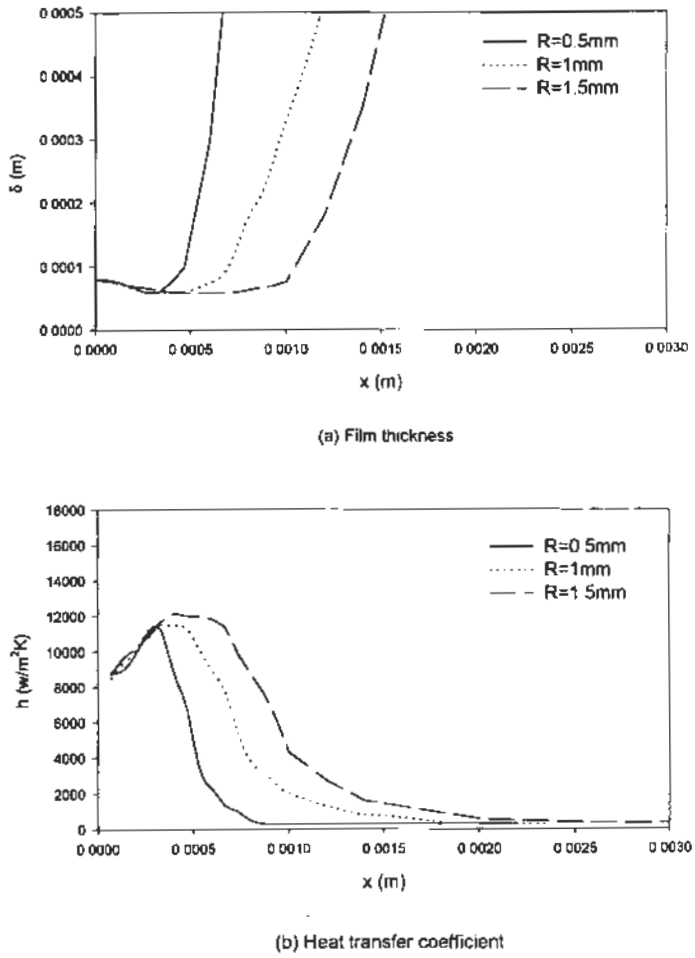

Figure 15. Effect of the distance between parallel plates on condensation ($T_{sat} = 363K$, $T_w = 340K$)

tension increases, the liquid film thickness up to the blocking point decreases and the condensation length decreases for both the tube and parallel plates. The liquid film thickness and the condensation length decrease with decreasing channel sizes. When the total mass flow rate decreases, the liquid film thickness increases and the condensation length decreases.

ACKNOWLEDGMENT

Funding for this work was provided by NASA Grant NAG3-1870 and NSF Grant CTS 9706706.

REFERENCES

Barnea, D., Luninski, Y., and Taitel, Y., 1983, Flow Pattern in Horizontal and Vertical Two Phase Flow in Small Diameter Pipes, *Canadian Journal of Chemical Engineering*, Vol. 61, pp. 617-620.

Basu, B., and Srinivasan, J., 1988, Numerical Study of Steady State Laser Melting Problem, *Int. J. Heat Mass Transfer*, Vol. 31, pp. 2331-2338.

Begg, E, Khrustalev, D., and Faghri, A., 1999, Complete Condensation of Forced Convection Two-Phase Flow in a Miniature Tube, *Proceeding of 1998 International Mechanical Engineering Congress and Exposition*, Anaheim, CA, also in *ASME Journal of Heat Transfer*, Vol. 121 (to appear).

Brackbill, J.U., Kothe, D.B., and Zemach, C., 1992, A Continuum Method for Modeling Surface Tension, *Journal of Computational Physics*, Vol. 100, pp. 335-354.

Collier, J.G., and Thome, J.R., 1994, *Convective Boiling and Condensation*, Third Edition, Oxford University Press, New York.

Faghri, A., 1995, *Heat Pipe Science and Technology*, Taylor and Francis, Washington, DC.

Faghri, A., 1996, Heat Pipe Simulation, From Promise to Reality, *Procs. of 5th International Heat Pipe Symposium*, pp. 1-21, Melbourne, Australia, Nov. 17-20, 1996.

Faghri, A., 1999, Recent Advances and Challenges in Micro/Miniature Heat Pipes, *Procs. of 11th International Heat Pipe Conference*, Tokyo, Japan, Sep. 12-15,1999.

Fluent Inc., 1998, Fluent 4.5, User's Guide, Lebanon, NH.

Ganesh, R.K., Faghri, A., and Hahn, Y., 1997a, A generalized thermal modeling for laser drilling process, Part I - Mathematical Modeling & Numerical Methodology, *Int. J. Heat Mass Transfer*, Vol. 40, pp. 3351-3360.

Ganesh, R.K., Faghri, A., and Hahn, Y., 1997b, A generalized Thermal Modeling for Laser Drilling process, Part II - Numerical Simulation & Results, *Int. J. Heat Mass Transfer*, Vol. 40, pp. 3361-3373.

Harley, C., and Faghri, A., 1994, Complete Transient Two-Dimensional Analysis of Two-Phase Closed Thermosyphons Including the Falling Condensate Film, *ASME Journal of Heat Transfer*, Vol. 116, pp. 418-426.

Mandhane, J.M., Gregory, G.A., and Aziz, K., 1974, A Flow Pattern Map for Gas-Liquid Flow in Horizontal Pipes, *International Journal of Multiphase Flow*, Vol. 1, pp. 537-553.

Narain, A., Yu, G., and Liu, Q., 1997, Interfacial Shear Models and Their Required Asymptotic for Annular/Stratified Film Condensation Flows in Inclined Channels and Vertical Pipes, *International Journal of Heat and Mass Transfer*, Vol. 40, pp. 3559-3575.

Nichols, B.D., Hirt, C.W., and Hotchkiss, R.S., 1980, *SOLA-VOF: A Solution Algorithm for Transient Fluid Flow with Multiple Free Boundary*, Los Alamos Scientific Laboratory, LA-8355.

Patankar, S.V., 1980, *Numerical Heat Transfer and Fluid Flow*, Hemisphere, Washington, DC.

Seban, R.A., and Faghri, A., 1985, Film Condensation in a Vertical Tube with a Closed Top, *International Journal of Heat and Mass Transfer*, Vol. 27, pp. 944-948.

Shekriladze, I.G., and Gomelauri, V.I., 1966, Theoretical Study of Laminar Film Condensation of Flowing Vapour, *Int. J. Heat Mass Transfer*, Vol. 9, pp. 581-591.

Taitel, Y., and Dukler, A.E., 1976, A Model for Predicting Flow Regime Transitions in Horizontal and Near Horizontal Gas-Liquid Flow, *AIChE Journal*, Vol. 22, pp. 47-55.

Takata, Y., Shirakawa, H., Kuroki, T., and Ito, T., 1998, Numerical Analysis of Single Bubble Departure from a Heated Surface, *Heat Transfer 1998, Proceedings of 11th International Heat Transfer Conference*, Vol. 4, pp. 355-360.

Takata, Y., Shirakawa, H., Sasaki, H., Kuroki, T., and Ito, T., 1999a, Numerical Analysis of Rapid Solidification in a Single Roller Process, *Heat Transfer— Asian Research*, Vol. 28, pp. 34-49.

Takata, Y., Shirakawa, H., Kuroki, T., and Ito, T., 1999b, An Improved VOF Method and Its Application to Phase Change Problems, *Proceedings of the 5th ASME/JSME Joint Thermal Engineering Conference*, March 15-19, 1999, San Diego, CA.